CDF/ANAL/EXOTIC/PUBLIC//11103

Tests of the Spin and Parity of the Higgs Boson with CDF

The CDF Collaboration[1]

[1] *URL http://www-cdf.fnal.gov*

(Dated: September 14, 2014)

Abstract

We perform tests of the spin and parity of the Higgs boson using dedicated searches for two specific non-standard Higgs boson hypotheses: a pseudoscalar Higgs boson with $J^P = 0^-$ and a graviton-like Higgs boson, with $J^P = 2^+$, both assuming a boson mass $m_\phi = 125$ GeV. We search for these exotic states in the $W\phi \to \ell\nu b\bar{b}$, $Z\phi \to \ell^+\ell^- b\bar{b}$, and $(W\phi + Z\phi) \to \not\!\!E_T b\bar{b}$ modes, making use of expected kinematical differences between events containing exotic Higgs bosons and those containing Standard Model Higgs bosons. The data correspond to an integrated luminosity of 9.45 fb^{-1}. We observe no significant deviations in the data from the predictions of the Standard Model with a Higgs boson of mass $m_H \approx 125$ GeV, and set bounds on the possible rate of production of each exotic state, both allowing for an admixture of Standard Model production and exotic production, and assuming only exotic production.

INTRODUCTION

The observation of a narrow bosonic resonance H with mass near 125 GeV by the ATLAS [1] and CMS [2] collaborations in the $H \to \gamma\gamma$ and $H \to ZZ \to \ell^+\ell^-\ell^+\ell^-$ modes marks the beginning of a line of inquiry that tests the fundamentals of the Standard Model (SM) and many possible extensions of it. The properties of the new boson are consistent, within the measurement uncertainties, with those predicted for the SM Higgs boson. A SM Higgs boson of that mass is expected to have significant decay branching fractions to W^+W^-, $b\bar{b}$, $\tau^+\tau^-$, gg, $c\bar{c}$, and $\gamma\gamma$. It is expected to be produced at hadron colliders in the gluon fusion $gg \to H$ mode, the WH and ZH associated-production modes, the vector-boson-fusion mode $qq \to qqH$, and the $t\bar{t}H$ mode.

The prediction at the Tevatron for the production rate and decay branching ratios in the $WH + ZH$ modes with $H \to b\bar{b}$ gives CDF a sensitivity of approximately 1σ to a SM Higgs boson at $m_H = 125$ GeV [3]. The D0 experiment has similar sensitivity [4], and together with CDF, the observed candidates in this mode provided evidence for a SM-like Higgs boson [5]. These search channels therefore provide sensitivity for testing not only the presence of a new particle, but also its properties. Models with exotic couplings of the Higgs boson to other particles may enhance the production cross sections, the decay branching ratios, or the kinematic distributions of signal events. Studies of the couplings of the Higgs boson to other particles have been performed at the Tevatron by CDF [6] and D0 [7], and the combined results are given in Ref. [8].

The studies mentioned above are limited to models in which a scalar Higgs boson with modified coupling strengths compared to SM predictions is present. Other models allow for the new particle to have different spin and parity states. Because the new particle was detected in decays to pairs of bosons and there is evidence for its decay into pairs of fermions, the new particle is a boson. Its decay into $\gamma\gamma$ constrains it not to be a vector $J = 1$ particle [9, 10]. A pseudoscalar state $J^P = 0^-$ is allowed by the observed decays, as are higher spin states, such as $J^P = 2^+$. The ATLAS [11] and CMS [12] have tested several non-SM spin-parity hypotheses using the $H \to ZZ \to \ell^+\ell^-\ell^+\ell^-$, $H \to W^+W^- \to \ell^+\nu\ell^-\bar{\nu}$, and $H \to \gamma\gamma$ decay modes, with the conclusion that the minimal SM Higgs boson with $J^P = 0^+$ is favored over the exotic hypotheses.

It is predicted that the Tevatron can also test alternate J^P hypotheses in the WH, ZH production modes with $H \to b\bar{b}$ by examining the kinematic distributions of the observable decay products of the vector boson and the Higgs-like boson [13]. The models considered are described in more detail in Ref. [14]. For the SM case, $J^P = 0^+$, and the production is an s-wave process, with a cross section that rises proportional to β close to threshold, where β is the speed of the Higgs boson in the production center of mass frame. In the 0^- case, the production is p-wave, and the cross section rises proportional to β^3. There are several possible $J^P = 2^+$ models, but for the graviton-like one considered in Ref. [13], the production is a d-wave process, with a cross section that rises proportional to β^5. These modifications to the production matrix element have strong impacts on the observable kinematic distributions, particularly $M(Vb\bar{b})$. The average value of $M(Vb\bar{b})$ is much larger in the 2^+ case than it is for the 0^+ case, and the 0^- case is intermediate between the other two. This difference in kinematics is also seen in other variables that are correlated with $M(Vb\bar{b})$, such as $\not\!\!E_T$ in the $ZX \to \nu\bar{\nu}b\bar{b}$ decays. Because CDF's $\not\!\!E_T$ trigger is more efficient for larger values of $\not\!\!E_T$, the $WX, ZX \to \not\!\!E_T b\bar{b}$ search has a higher acceptance for the two exotic signals than it has for the SM Higgs signal. The other two channels which trigger on one or both leptons, have a milder dependence on the $\not\!\!E_T$ distribution.

The models studied in Ref. [13] do not predict the production cross sections for $p\bar{p} \to WH, ZH$, nor the decay branching fraction $B(H \to b\bar{b})$. Instead, it is suggested to purify a sample of Higgs boson candidate events, and to study the invariant mass of the $Wb\bar{b}$ and $Zb\bar{b}$ systems, which differ strongly between the 0^+, 0^-, and 2^+ models. A similar strategy works well at the LHC in the $H \to ZZ \to \ell^+\ell^-\ell^+\ell^-$ mode, as a sample of Higgs boson candidate events with a signal-to-background ratio of approximately 2:1 can be purified with data selection criteria that minimally bias the kinematic properties that are sensitive to the spin and parity of the parent boson.

This situation is not the case at the Tevatron, however, with a typical signal-to-background ratio for a SM Higgs of $\approx 2\%$. (This is the approximate signal-to-background ratio in CDF's $WH \to \ell\nu b\bar{b}$ search with two jets and two tight b-tags [15].) With the use of mutivariate analyses (MVA's), small subsets of the data sample can be purified with a signal-to-background ratio of $\approx 1:1$ are obtained. Since these events are selected with MVA discriminants that are functions of the kinematic properties of the signals and backgrounds, the distributions of the small numbers of events thus selected are highly sculpted to resemble

TABLE I: The production cross sections and decay branching fraction for the SM Higgs boson assumed for the combination, evalulated at $m_H = 125$ GeV/c^2.

σ_{WH}	129.5 fb
σ_{ZH}	78.5 fb
$Br(H \to b\bar{b})$	57.8%

those predicted by the SM Higgs boson, and thus are not expected to be optimal in testing alternate models.

The strategy chosen for this paper is to generalize the searches for the SM Higgs boson at CDF in the $WH \to \ell\nu b\bar{b}$ [15] mode, the $ZH \to \ell^+\ell^- b\bar{b}$ [16], and the $WH + ZH \to \not\!\!E_T b\bar{b}$ [17] mode to also search for pseudoscalar ($J^P = 0^-$) and graviton-like ($J^P = 2^+$) bosons, using the MVA techniques developed for the SM search. Admixtures of SM and exotic Higgs particles with indistinguishable mass are also considered. We set limits on the production cross sections times the branching ratios of $H \to b\bar{b}$, as well as perform hypothesis tests of the exotic models by comparing the consistency of the data with the SM prediction and the consistency of the data with the prediction assuming an exotic boson is present with production cross sections and decay branching ratios as predicted by the SM, and also as measured in the SM Higgs boson search.

SIGNAL MODELS

To predict the kinematic distributions of Higgs boson signal events, we use the PYTHIA [18] Monte Carlo program, with CTEQ5L [19] leading-order (LO) parton distribution functions (PDFs). We scale these Monte Carlo predictions to the highest-order cross section calculations available.

The predictions for the WH and ZH cross sections are taken from Ref. [20]. This calculation starts with the NLO calculation of V2HV [21] and includes NNLO QCD contributions [22], as well as one-loop electroweak corrections [23]. A similar calculation of the WH cross section is available in Ref. [24].

We use the predictions for the branching ratios of the Higgs boson decay from Refs. [25, 26]. In this calculation, the partial decay widths for all Higgs boson decays except to pairs of W and Z bosons are computed with HDECAY [27], and the W and Z pair decay widths are computed with PROPHECY4F [28]. The relevant cross sections and decay branching ratio are listed in Table I. The uncertainties on the predicted branching ratio from uncertainties in the charm- and bottom-quark masses, α_s, and missing higher-order effects are presented in Refs. [29],[30].

BACKGROUND MODEL

We model SM and instrumental background processes using a mixture of Monte Carlo (MC) and data-driven methods. Diboson (WW , WZ , ZZ) MC samples are normalized using the NLO calculations from MCFM [31]. For $t\bar{t}$ we use a production cross section of 7.04 ± 0.7 pb [32], which is based on a top-quark mass of 173 GeV/c^2 and MSTW 2008 NNLO PDFs [33]. The single-top-quark production cross section is taken to be 3.15 ± 0.31 pb [34]. The normalization of the Z+jets and W+jets MC samples is taken from ALPGEN [35] corrected for NLO effects, except in the case of the $WH \to \ell\nu b\bar{b}$ search. The normalization of the W+jets MC sample in the $WH \to \ell\nu b\bar{b}$ search, and normalization of the instrumental and QCD multi-jet samples in all searches, are constrained from data samples where the expected signal is several orders of magnitude smaller than in the search samples.

SEARCH CHANNELS

The analyses used to search for the exotic graviton-like and pseudoscalar Higgs bosons are versions of the analyses used to search for the SM Higgs boson, optimized for separating the exotic signals from both the SM background sources and the possible SM Higgs boson signal. The channels used here assume that the exotic particle is produced in association with a vector boson and decays $X \to b\bar{b}$. The vector boson is either W or Z, and leptonic decays of the vector boson, including the invisible decay $Z \to \nu\bar{\nu}$ are used, in order to separate the signal from large QCD backgrounds.

Because the X particle is expected to decay to $b\bar{b}$, the searches use CDF's most sensitive b-tagging algorithm, HOBIT [36], a multivariate classifier which uses kinematic properties of tracks associated with displaced vertices, the impact parameters of the tracks, and other characteristics of reconstructed jets that help separate b-jets from light-flavored jets. The channels listed here use the same *tight* and *loose* operating points for the HOBIT tagger used in the corresponding SM Higgs boson searches. For b jets from Higgs boson decay, the tagging efficiency of HOBIT is roughly 20% higher than the older SECVTX [37] algorithm at the same light-flavor tag rate. Because HOBIT was optimized using the SM Higgs boson as the target signal, it is most sensitive in the kinematic range populated by that signal. SM Higgs boson decays very seldom give rise to b jets with $E_{\rm T} > 200$ GeV, and the sample of jets in the data used to validate the b-tagging efficiency and mistag rates is likewise small and its composition is uncertain. We therefore do not use the HOBIT tagger to tag jets with $E_{\rm T} > 200$ GeV, even though the exotic signals sought here give rise to jets with that energy rather frequently. This choice reduces the acceptance of the b-tagged event selection, more for the 2^+ signal than the 0^- or SM Higgs signals. This loss of acceptance is partially counteracted by the fact that more jets pass the lower cut on $E_{\rm T}$, and cuts on $\not\!\!E_T$ are also satisified more frequently by the exotic signals than the SM signals.

The search channels focus on reconstructed final states – $WX \to \ell\nu b\bar{b}$ [15], $ZX \to \ell^+\ell^- b\bar{b}$ [16], and $WX + ZX \to \not\!\!E_T b\bar{b}$ [17]. Sub-dominant contributions to the signal from associated production modes are also included. For example, $ZX \to \ell^+\ell^- b\bar{b}$ events may be reconstructed as $\not\!\!E_T b\bar{b}$ events if both leptons fail to be identified. In each of the final states listed above, the channels are further sub-divided by the number of jets, the lepton category, and the b-tag category. The expected and observed event yields in all channels are summarized in Table II.

CANDIDATE DISTRIBUTION

The number of contributing channels is large, and their sensitivity varies from one final state to another and on their event classification. The discriminating variables chosen and their binning are also not commensurate from one channel to another, and so the distributions cannot be simply summed. If the distributions were summed, then the channels with large backgrounds will dominate the sum and the signal will not be easily visible. To address

TABLE II: Expected and observed event yield summary for all channels.

Process	$\ell^+\ell^- b\bar{b}$	$\ell\nu b\bar{b}$	$\not\!\!E_T b\bar{b}$
V+Graviton	7±1	43±3	65±5
V+Pseudoscalar	8±1	49±3	81±5
VH	7±1	33±2	40±2
V+jets	820±141	23323±2077	9193±1435
Dibosons	72±7	1288±79	544±26
Top	222±22	2053±119	1935±128
QCD	58±22	2406±603	16283±1220
Total Bkg	1172±199	29070±2331	27956±3027
Data	1182	26337	28518

these issues, we follow the procedure used in Ref [8] to visualize the aggregate data from the contributing channels. Bins with similar signal to background ratios (s/b) are aggregated together from all contributing sub-channels, and the data are displayed compared with the signal and background predictions. The distributions are shown separately for the 2^+ search and the 0^- search in Figure . The backgrounds are fit to the data in each case, allowing the systematic uncertainties to float. For symmetry, neither the SM Higgs boson signal nor the exotic signal is included in these fits. The exotic signal, within the a priori constraints, is shown stacked, and the SM signal is shown as a separate, unstacked histogram. The sorting of the bins is performed using the ratio of the predicted exotic signal to the predicted background. Both signals are shown assuming $\mu_{\text{exotic}} = \mu_{\text{SM}} = 1$, where μ_{exotic} (μ_{SM}) is the scaling factor applied to the exotic (SM) Higgs boson signal. This representation of the data is not used to compute the final results, since the distribution indiscriminately sums unrelated backgrounds which are fit separately. It does, however, provide a guide to how much individual events contribute to the results and how well the signal is separated from backgrounds in the combined search. Both distributions show agreement between the background predictions and the observed data over five orders of magnitude, and no evidence for an excess of exotic signal-like candidates.

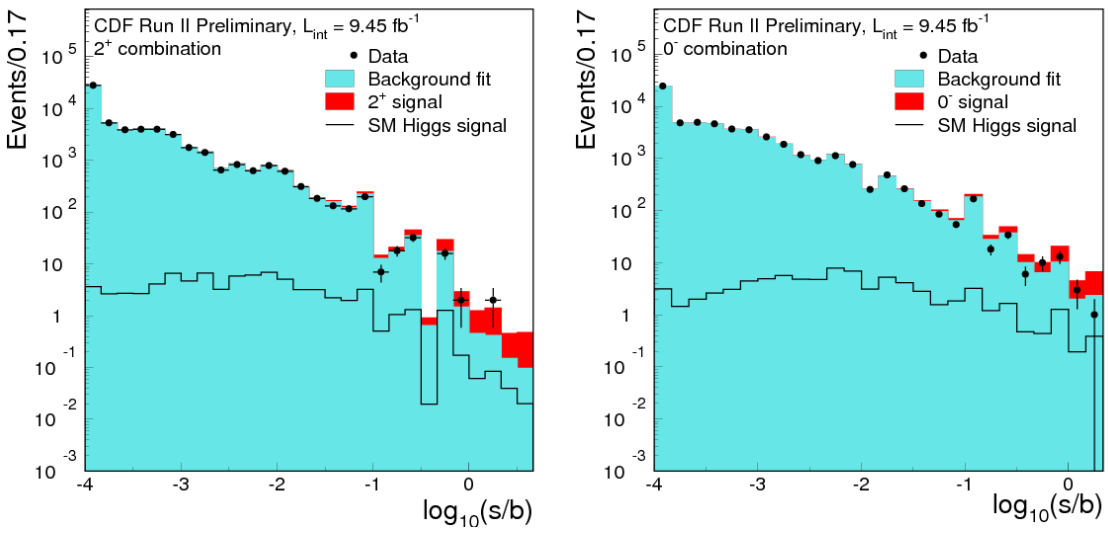

FIG. 1: Distributions of $\log_{10}(s/b)$, for the data from all contributing Higgs boson search channels for $m_H = 125$ GeV/c^2 for the 2^+ search (left-hand plot) and the 0^- search (right-hand plot). The data are shown with points, and the expected exotic signals are shown with $\mu_{\rm exotic} = 1$ stacked on top of the backgrounds, which are fit to the data within their systematic uncertainties. The s/b used to rank analysis bins is the exotic signal divided by the background. The background predictions do not include the contributions from the SM Higgs boson, which are shown as separate histograms, not stacked. The error bars shown on the data correspond in each bin to the square root of the observed data count. Underflows and overflows are collected into the leftmost and rightmost bins, respectively.

We also display in Figure the data distributions sorted by the ratio of the exotic signal to the predicted background, with the background subtracted. Wider bins are chosen than in Figure , and underflows and overflows are collected into the lowest and highest visible bins, respectively. As in Fig. , the background-only model has been fit to the data, allowing the systematic uncertainties to float. The signals are shown assuming $\mu_{\rm exotic} = \mu_{\rm SM} = 1$; the post-fit uncertainties on the background are also displayed. No excess of data is seen above the background fits in the bins most sensitive to an exotic signal.

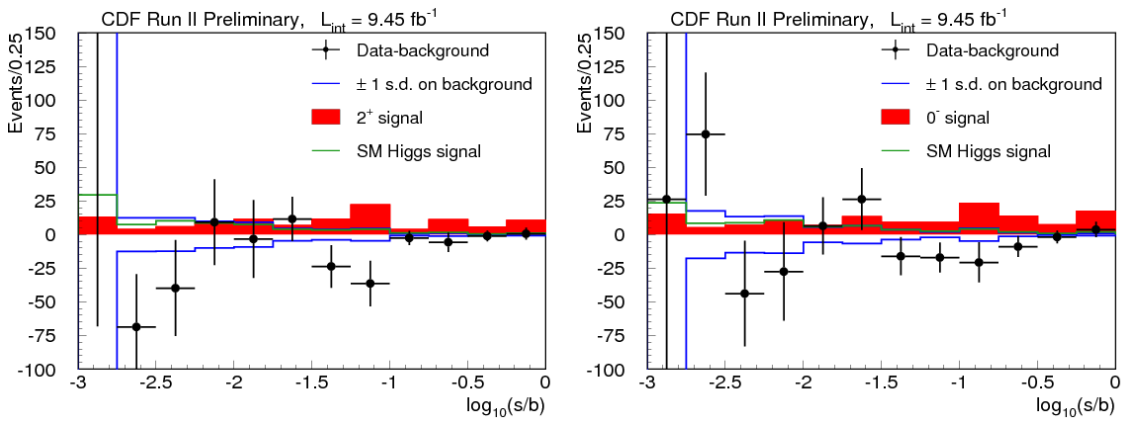

FIG. 2: Background-subtracted distribution of the discriminant histograms, summed for bins with similar signal-to-background ratio (s/b) over all contributing Higgs boson search channels, for $m_H = 125$ GeV/c^2, for the 2^+ search (left-hand plot) and the 0^- search (right-hand plot). The background is fit to the data in each case, and the uncertainty on the background, shown with dashed lines, is after the fit. The exotic signal model, scaled to the SM Higgs boson expectation, is shown with a filled histogram. The SM Higgs boson expectation is also shown with a solid line. The error bars shown on the data points correspond in each bin to the square root of the sum of the expected signal and background yields. Underflows and overflows are collected into the leftmost and rightmost bins, respectively.

STATISTICAL TECHNIQUES

We interpret the results of the searches by computing exclusion limits, cross section fits, and p values for testing the graviton and pseudoscalar hypotheses. The first step in all of our interpretations is the construction of a binned likelihood, combined for all contributing channels by multiplying the individual channels' likelihoods together. For a single channel, this likelihood is the product over the bins of the histogram of the MVA distribution of the Poisson proability for observing the data in that bin given the signal and background predictions, as a function of the nuisance parameters, which express our systematic uncertainties. The joint likelihood takes the form

$$L(\text{data}|\mu_{\text{SM}}, \mu_{\text{exotic}}, \vec{s_{\text{SM}}}, \vec{s_{\text{exotic}}}\vec{b}|\vec{n}, \vec{\theta}) \times \pi(\vec{\theta}) = \prod_{i=1}^{N_{\text{C}}} \prod_{j=1}^{N_{\text{bins}}} r_{ij}^{n_{ij}} \frac{e^{-r_{ij}}}{n_{ij}!} \times \prod_{k=1}^{n_{\text{sys}}} e^{-\theta_k^2/2}. \quad (1)$$

In this expression, the first product is over the number of channels (N_{C}), and the second product is over histogram bins containing n_{ij} events, binned in ranges of the final discrim-

inant variables used for the individual analyses. The predictions for the bin contents are $r_{ij} = \mu_{\rm SM} \times s_{{\rm SM},ij}(\vec{\theta}) + \mu_{\rm exotic} \times s_{{\rm exotic},ij}(\vec{\theta}) + b_{ij}(\vec{\theta})$ for channel i and histogram bin j, where $s_{{\rm SM},ij}$, $s_{{\rm exotic},ij}$, and b_{ij} represent the expected SM Higgs boson signal, the exotic Higgs boson signal, and the SM background in the bin, respectively, and $\mu_{\rm SM}$ ($\mu_{\rm exotic}$) is the scaling factor applied to the SM (exotic) Higgs boson signal. By scaling all SM Higgs boson signal contributions by the same factor, we assume that the relative contributions of the different processes are as given by the SM. We also assume the SM production and decay ratios for the exotic Higgs boson, which is a mild assumption since all channels reported here are sensitive only to $X \to b\bar{b}$ and the ratios of associated production with a W and a Z are likely to be close to those in the SM due to custodial symmetry.

Systematic uncertainties are parametrized by the dependence of $s_{\rm SM,ij}$, $s_{\rm exotic,ij}$, and b_{ij} on $\vec{\theta}$. Each of the $n_{\rm sys}$ components of $\vec{\theta}$, θ_k, corresponds to a single independent source of systematic uncertainty, and each parameter may have an impact on several sources of signal and background in different channels, thus accounting for correlations. Gaussian priors are assumed for the θ_k, truncated so that no prediction is negative.

To compute the exclusion limits and the best-fit cross sections, we adopt a Bayesian approach. In these calculations, likelihood function, multiplied by the θ_k priors, $\pi(\theta_k)$, is then integrated over θ_k including correlations [38],

$$L'({\rm data}|\mu_{\rm SM}, \mu_{\rm exotic}) = \int L({\rm data}|\mu_{\rm SM}, \mu_{\rm exotic}, \vec{s}, \vec{b}|\vec{n}, \vec{\theta})\pi(\vec{\theta})d\vec{\theta}. \quad (2)$$

To compute upper limits on the rate of exotic Higgs boson production, We assume a uniform prior in $\mu_{\rm exotic}$ and obtain its posterior distribution. The observed 95% credibility upper limit on $\mu_{\rm exotic}$, $\mu_{{\rm exotic},95^{\rm obs}}$ satisfies $0.95 = \int_0^{\mu^{\rm obs}_{{\rm exotic},95}} L'(\mu_{\rm exotic}){\rm d}\mu_{\rm exotic}$. The expected distribution of $\mu_{\rm exotic,95}$ is computed in an ensemble of pseudoexperiments generated without exotic signal. In each pseudoexperiment, random values of the nuisance parameters are drawn from their priors. The median expected value of $\mu_{\rm exotic,95}$ in this ensemble is denoted $\mu^{\rm exp}_{\rm exotic,95}$. The observed and expected upper limits on $\mu_{\rm exotic}$ are computed separately assuming the presence of a Higgs boson with SM properties, and also assuming its absence. The upper limits are computed separately for graviton-like and pseudoscalar Higgs bosons. These observed and expected limits are listed for each channel and their combinations in Tables III, IV, V, VI.

We also perform two-dimensional cross section fits, allowing for the possibility of an arbitrary admixture of SM-like and exotic Higgs bosons. Assuming a uniform prior in the (μ_{SM}, μ_{exotic}) plane, we compute the posterior probability density for each of the input channels and their combination, separately for the graviton-like and pseudoscalar exotic Higgs boson hypotheses. Figures 1 through 4 show the smallest two-dimensional domains integrating 68% and 95% of the posterior probability densities. The point in the (μ_{SM}, μ_{exotic}) plane which maximizes the posterior probability density is shown as the best fit value.

We also compute p values for the discrete two-hypothesis tests, with the SM Higgs boson hypothesis on one hand, and the exotic hypothesis on the other. Because there is no theoretical prediction for the production cross sections and decay branching ratios, we choose to test the model (μ_{SM}=0, μ_{exotic}=1) against the model (μ_{SM}=1, μ_{exotic}=0). The test statistic used to compute these p values is the ratio of maximized likelihoods, shown here for the first case above, testing

$$\mathrm{LLR} = -2\ln\left(\frac{L(\mathrm{data}|\mu_{\mathrm{SM}}=0,\mu_{\mathrm{exotic}}=1,\hat{\theta})\pi(\hat{\theta})}{L(\mathrm{data}|\mu_{\mathrm{SM}}=1,\mu_{\mathrm{exotic}}=0,\hat{\hat{\theta}})\pi(\hat{\hat{\theta}})}\right) \tag{3}$$

where $\hat{\theta}$ are the best-fit values of the nuisance parameters assuming the exotic Higgs boson hypothesis, and $\hat{\hat{\theta}}$ are the best-fit values assuming the SM Higgs boson hypothesis.

To compute the p values, pseudoexperiments are drawn either from the SM Higgs boson hypothesis or the exotic Higgs boson hypothesis, where values of the nuisance parameters are drawn randomly from their prior distributions. We compute two p values, which test either the SM hypothesis (p_{null}) or the exotic hypothesis (p_{test}). These are defined as

$$p_{\mathrm{null}} = P(\mathrm{LLR} \leq \mathrm{LLR}_{\mathrm{obs}}|\mathrm{SM}), \tag{4}$$

and

$$p_{\mathrm{test}} = P(\mathrm{LLR} \geq \mathrm{LLR}_{\mathrm{obs}}|\mathrm{exotic}). \tag{5}$$

A small value of p_{null} is the customary criterion for claiming evidence (with a threshold of 0.00135) or observation (with a threshold of 2.87×10^{-7}) of a new particle or process. A small value of p_{test} (typically 0.05) is used to exclude the test hypothesis. In order to prevent exclusion of models for which there is insufficient sensitivity, due to a downward fluctuation in the background, we also quote the values of

$$\mathrm{CL_s} = p_{\mathrm{test}}/(1 - p_{\mathrm{null}}). \tag{6}$$

Table VII lists the observed and the median expected values of $p_{\rm null}$, $p_{\rm test}$, and $\rm CL_s$ separately for each channel and combined, for the graviton-like and pseudoscalar hypotheses, assuming $\mu_{\rm exotic}$=1. The median expected $p_{\rm null}$ values are computed assuming an exotic signal is present, and the median expected $p_{\rm test}$ and $\rm CL_s$ values are computed assuming the exotic signal is absent but a SM signal is present. In order to compute the very small values of $p_{\rm test}$ and the expected values of $p_{\rm null}$ and $p_{\rm test}$, each distribution of LLR is fit to a sum of two Gaussian distributions and the tails of the double Gaussian are integrated to compute the p values. Table VII also lists the equivalent number of Gaussian standard deviations z corresponding to each p value, using the one-sided definition

$$p = (1 - \mathrm{erf}(z/\sqrt{2}))/2. \tag{7}$$

SYSTEMATIC UNCERTAINTIES

Though many sources of systematic uncertainty differ among the analyses, all correlations are taken into account in the combined limits, cross sections, and p-values. The uncertainties on the signal production cross sections are estimated from the factorization and renormalization scale variations, which includes the impact of uncalculated higher-order corrections, uncertainties due to PDFs, and the dependence on the strong coupling constant, (α_s). The resulting uncertainties on the inclusive WH and ZH production rates are 5% [20, 39]. We assign uncertainties to the Higgs boson decay branching ratios as calculated in Ref. [30]. These uncertainties arise from imperfect knowledge of the mass of the b and c quarks, α_s, and theoretical uncertainties in the $b\bar{b}$ decay rates. The largest sources of uncertainty on the dominant backgrounds in the b-tagged channels are the rates of V+heavy flavor jets, where $V = W$ or Z, which are typically 30% of the predicted values. The posterior uncertainties on these rates are typically 8% or less. Because the different analyses use different methods to obtain the V+heavy flavor predictions, we treat their uncertainties as uncorrelated between the $\ell\nu b\bar{b}$, the $\not\!\!E_T b\bar{b}$, and $\ell^+\ell^- b\bar{b}$ channels. We use simulated events to study the impact of the jet energy scale uncertainty [40] on the rates and shapes of the signal and background expectations. We observe that the jet energy scale uncertainty is highly constrained by the data in the individual channels. Because differences between channels in the event selection and modeling of the background shapes affect the constraint on the jet energy scale obtained

from the fit, we conservatively choose to treat the jet energy scale variations uncorrelated between the three analyses in the combined search.

Uncertainties on lepton identification and trigger efficiencies range from 2% to 6% and are applied to both signal- and MC-based background predictions. The uncertainty on the integrated luminosity of 6% arises from uncertainties in the luminosity monitor acceptance and the inelastic $p\bar{p}$ cross section [41], and is assumed to be correlated between the signal- and MC-based background predictions.

RESULTS

Limits on the production rates times the decay branching fraction $Br(X \to b\bar{b})$ for 0^- and 2^+ Higgs bosons are reported, separately for each channel and combined, in Tables III, IV, V, VI. The results are reported in units of the SM Higgs boson production rate. The signal strength modifier is denoted by μ_{exotic} which multiplies the SM signal strength to predict the rate in the exotic model under test. The SM ratio between WH and ZH production is assumed when combining searches for WX and ZX. Limits are listed either assuming the SM Higgs boson is present as a background, or absent. Because the exotic 0^- and 2^+ signals populate different kinematic regions from the SM Higgs boson, and because the SM Higgs boson production rate is small, the expected and observed limits on the exotic rates are very similar whether a SM Higgs boson is present or not. The observed combined limits are somewhat stronger than expected, with an exclusion rate of $\mu_{\text{exotic}} < 0.24$ in the 2^+ case (approximately a two standard deviation deficit), and $\mu_{\text{exotic}} < 0.32$ in the 0^- case (approximately a one standard deviation deficit). The $\not\!\!E_T b\bar{b}$ channel dominates in the combination, and a somewhat lower than expected number of data candidates appear in the highest-score bins of the exotic discriminants in this channel.

The two-dimensional cross section fits, which allow for arbitrary rates of both SM and exotic Higgs bosons to be simultaneously present in the data, are shown in Figs. 1 through 4, for each channel and combined, and separately for the 0^- and 2^+ searches. The combined results do not show evidence for an exotic Higgs boson and are consistent with the presence of the SM Higgs boson at the predicted rate. Because the discriminants used in this analysis have been optimized to search for the 0^- and 2^+ search, we do not expect the same sensitivity or the same result for the SM Higgs boson fit cross section in CDF's SM Higgs boson

TABLE III: CDF Graviton Limits, assuming no SM Higgs boson background.

Channel	obs (Limit/SM)	-2σ exp (Limit/SM)	-1σ exp (Limit/SM)	Median exp (Limit/SM)	$+1\sigma$ exp (Limit/SM)	$+2\sigma$ exp (Limit/SM)
CDF $\ell\nu b\bar{b}$	1.05	0.55	0.73	1.01	1.42	1.99
CDF $\ell^+\ell^- b\bar{b}$	1.57	0.87	1.16	1.59	2.18	2.95
CDF $\not\!\!E_T b\bar{b}$	0.41	0.42	0.56	0.79	1.12	1.57
CDF Combined	0.35	0.29	0.39	0.54	0.75	1.04

TABLE IV: CDF Graviton Limits, assuming SM Higgs boson background.

Channel	obs (Limit/SM)	-2σ exp (Limit/SM)	-1σ exp (Limit/SM)	Median exp (Limit/SM)	$+1\sigma$ exp (Limit/SM)	$+2\sigma$ exp (Limit/SM)
CDF $\ell\nu b\bar{b}$	0.99	0.58	0.75	1.03	1.48	2.11
CDF $\ell^+\ell^- b\bar{b}$	1.49	0.92	1.18	1.61	2.25	3.15
CDF $\not\!\!E_T b\bar{b}$	0.37	0.45	0.60	0.83	1.15	1.58
CDF Combined	0.31	0.30	0.40	0.56	0.78	1.08

searches [6]. Indeed, because the kinematic distributions of the SM Higgs boson signal and the exotic signals are so different, the expected Higgs boson signal events populate different bins in the discriminants from those most sensitive to the exotic signals.

TABLE V: CDF Pseudoscalar Limits, assuming no SM Higgs boson background.

Channel	obs (Limit/SM)	-2σ exp (Limit/SM)	-1σ exp (Limit/SM)	Median exp (Limit/SM)	$+1\sigma$ exp (Limit/SM)	$+2\sigma$ exp (Limit/SM)
CDF $\ell\nu b\bar{b}$	0.59	0.39	0.53	0.74	1.04	1.43
CDF $\ell^+\ell^- b\bar{b}$	1.86	0.79	1.04	1.46	2.09	2.99
CDF $\not\!\!E_T b\bar{b}$	0.49	0.34	0.48	0.68	0.96	1.32
CDF Combined	0.32	0.24	0.32	0.44	0.62	0.87

TABLE VI: CDF Pseudoscalar Limits, assuming SM Higgs boson background.

Channel	obs (Limit/SM)	-2σ exp (Limit/SM)	-1σ exp (Limit/SM)	Median exp (Limit/SM)	$+1\sigma$ exp (Limit/SM)	$+2\sigma$ exp (Limit/SM)
CDF $\ell\nu b\bar{b}$	0.55	0.42	0.56	0.78	1.09	1.51
CDF $\ell^+\ell^- b\bar{b}$	1.77	0.82	1.08	1.52	2.18	3.10
CDF $\not\!\!E_T b\bar{b}$	0.43	0.36	0.50	0.69	0.96	1.31
CDF Combined	0.28	0.24	0.32	0.45	0.63	0.87

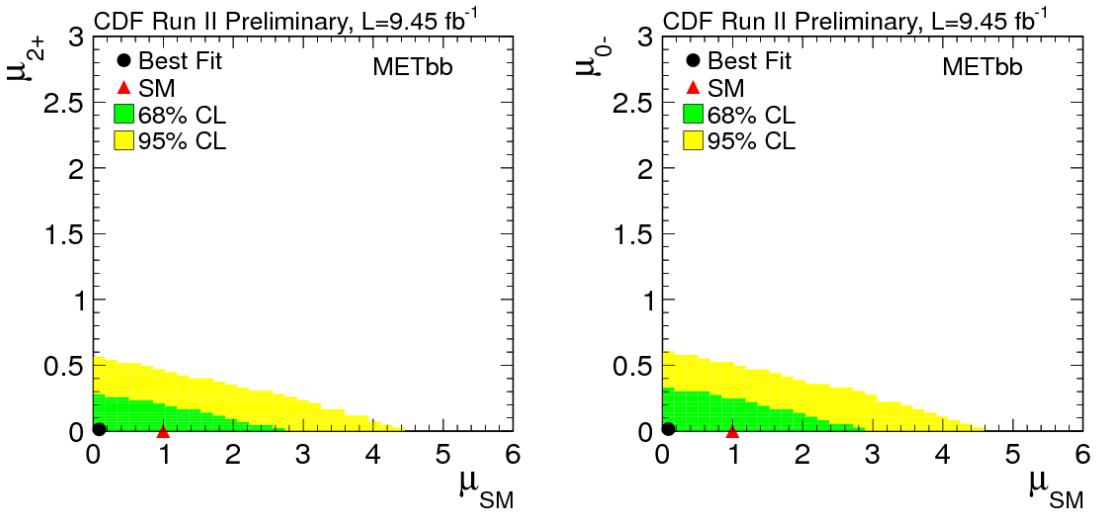

FIG. 3: $\not\!\!E_T b\bar{b}$ two-dimensional posterior density of the measured 2^+-vs.-0^+ (left), and 0^--vs.-0^+ (right) cross sections, normalized to the SM predictions.

We report the observed values and the expected distributions of LLR in the SM and the exotic hypotheses, and show the results in Figs. 5 through 8, and list the combined results in Table VII. The LLR test statistic ranks experimental outcomes along a spectrum of those that favor the exotic Higgs model, each chosen with a specific μ_{exotic} with a value 1.0.The deficit of data in the high-score bins of the exotic discriminant in the $\not\!\!E_T b\bar{b}$ channel results in a very non-exotic-Higgs outcome, in both the 0^- and the 2^+ searches, as is visible in Fig. 5, which is the dominant contribution to the combined result, shown in Fig. 8. The significance of the deficit is roughly 1.88 standard deviations for the 2^+ Higgs boson search, as listed in Table VII. This deficit in the exotic search is not evidence against the SM Higgs boson, as the exotic search tests for events with different kinematic properties (high $M_{Vb\bar{b}}$)

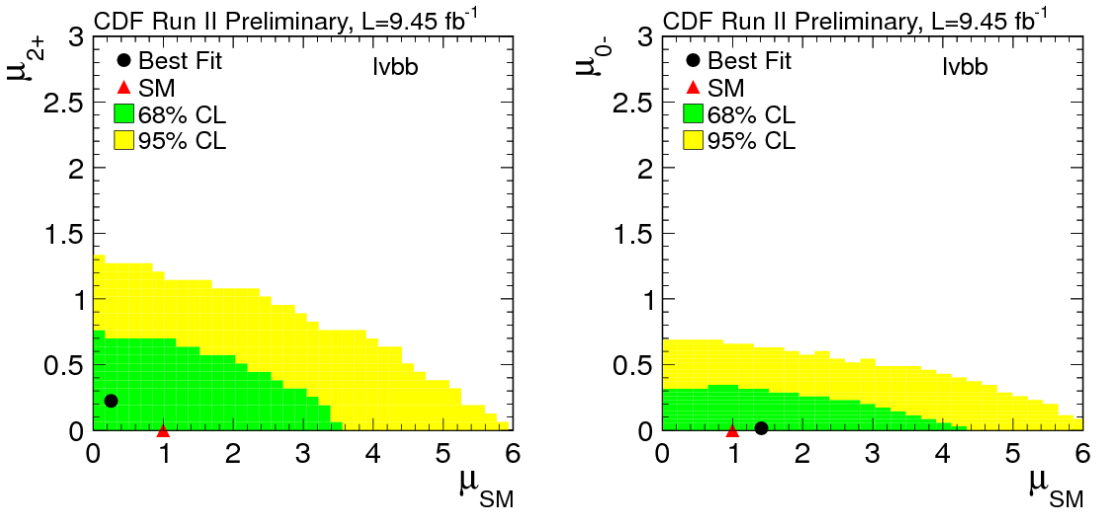

FIG. 4: $\ell\nu b\bar{b}$ two-dimensional posterior density of the measured 2^+-vs.-0^+ (left), and 0^--vs.-0^+ (right) cross sections, normalized to the SM predictions.

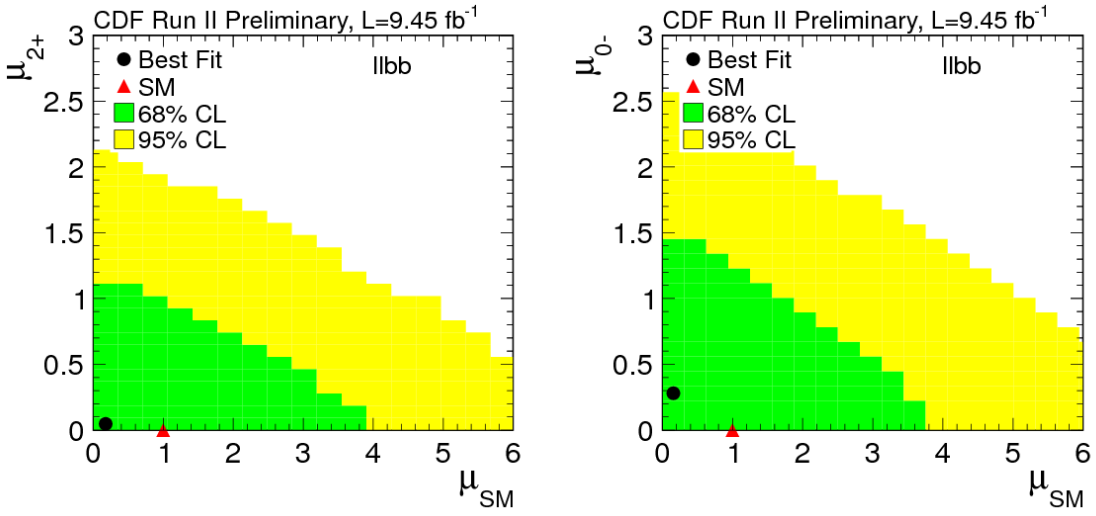

FIG. 5: $\ell\ell b\bar{b}$ two-dimensional posterior density of the measured 2^+-vs.-0^+ (left), and 0^--vs.-0^+ (right) cross sections, normalized to the SM predictions.

than those of the SM Higgs boson. Indeed, the combined cross section fit, shown in Fig. 4, is consistent with the SM Higgs boson rate with a discrepancy of less than 0.5 standard deviations.

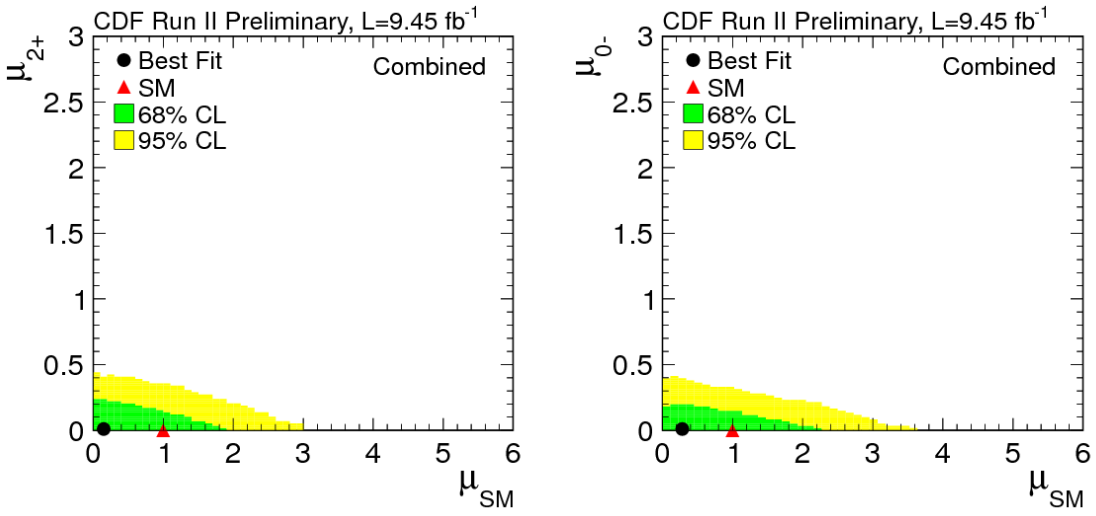

FIG. 6: CDF combined two-dimensional posterior density of the measured 2^+-vs.-0^+ (left), and 0^--vs.-0^+ (right) cross sections, normalized to the SM predictions.

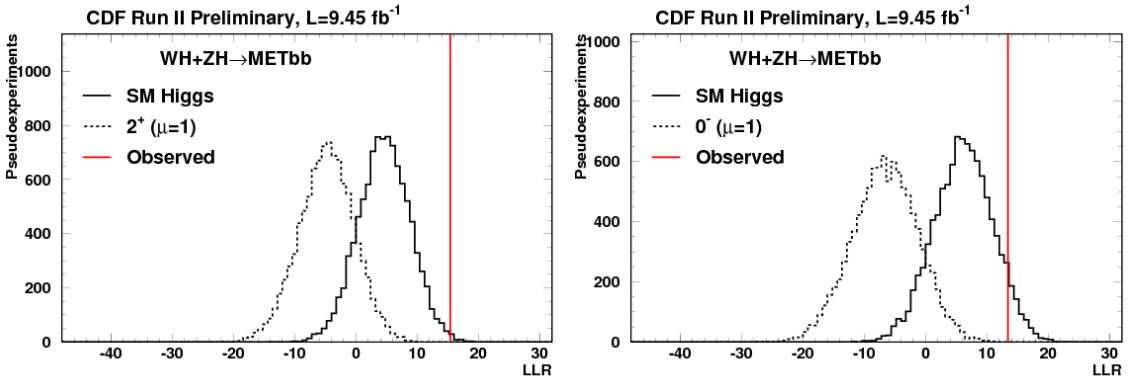

FIG. 7: $\not\!\!E_T b\bar{b}$ LLR distributions for 2^+ (left), and 0^- (right) hypotheses, assuming $\mu = 1$.

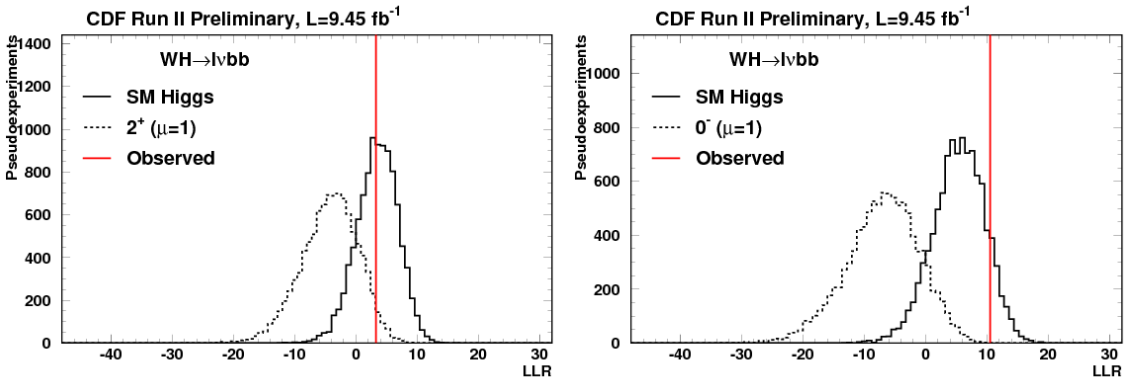

FIG. 8: $\ell\nu b\bar{b}$ LLR distributions for 2^+ (left), and 0^- (right) hypotheses, assuming $\mu = 1$.

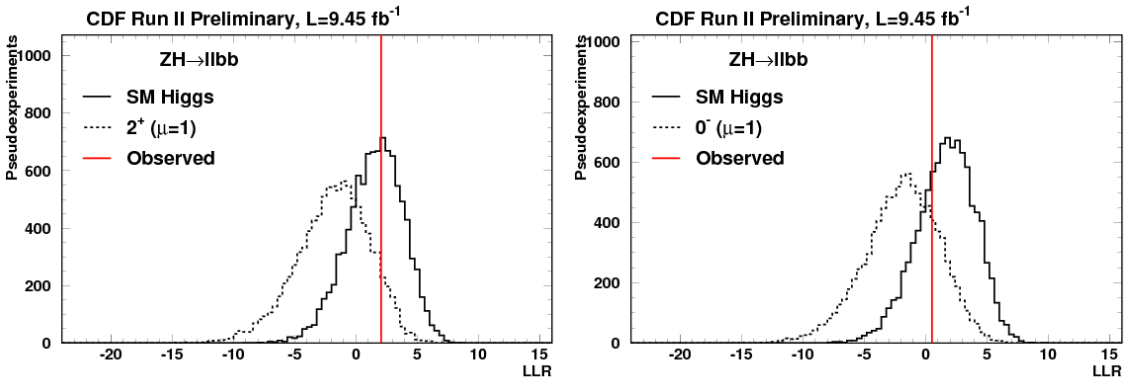

FIG. 9: $\ell\ell b\bar{b}$ LLR distributions for 2^+ (left), and 0^- (right) hypotheses, assuming $\mu = 1$.

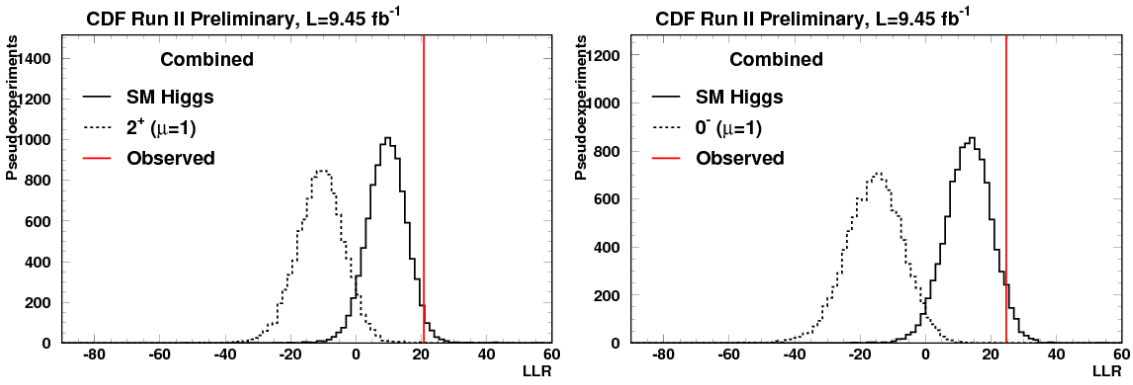

FIG. 10: CDF combined LLR distributions for 2^+ (left), and 0^- (right) hypotheses, assuming $\mu = 1$.

TABLE VII: LLR and p-values for the test hypotheses. The SM hypothesis includes a SM Higgs boson. The significances corresponding to the p values and CL_s are given in parentheses. The negative signal significance p_{null} is a reflection of the deficit of signal-like events compared with the background prediction.

	Graviton	Pseudoscalar
LLR_{obs}	20.8	24.6
$LLR_{SM,\ median}$	9.5	13.2
$LLR_{Grav,\ median}$	-10.8	-15.5
p_{null}	0.970 (-1.88 s.d.)	0.949 (-1.64 s.d.)
Median expected p_{null} (if exotic)	3.11×10^{-3} (2.74 s.d.)	7.74×10^{-4} (3.17 s.d.)
p_{test}	2.59×10^{-4} (3.47 s.d.)	5.96×10^{-6} (4.38 s.d.)
Median expected p_{test} (if SM)	3.73×10^{-3} (2.68 s.d.)	4.09×10^{-4} (3.35 s.d.)
CL_s	8.62×10^{-3} (2.38 s.d.)	1.17×10^{-4} (3.68 s.d.)
Median expected CL_s	7.47×10^{-3} (2.43 s.d.)	8.18×10^{-4} (3.15 s.d.)

SUMMARY

We performed a test of the spin and parity of the Higgs boson using CDF data. We observed no significant deviations from the SM predictions with a Higgs boson of mass $m_H \approx 125$ GeV, and set bounds on the possible rate of production of 2^+ and 0^- exotic state, both allowing for an admixture of Standard Model production and exotic production, and assuming only exotic production.

We thank the Fermilab staff and the technical staffs of the participating institutions for their vital contributions. This work was supported by the U.S. Department of Energy and National Science Foundation; the Italian Istituto Nazionale di Fisica Nucleare; the Ministry of Education, Culture, Sports, Science and Technology of Japan; the Natural Sciences and Engineering Research Council of Canada; the National Science Council of the Republic of China; the Swiss National Science Foundation; the A.P. Sloan Foundation; the Bundesministerium für Bildung und Forschung, Germany; the Korean World Class University Program, the National Research Foundation of Korea; the Science and Technology Facilities Council and the Royal Society, United Kingdom; the Russian Foundation for Basic Research; the Ministerio de Ciencia e Innovación, and Programa Consolider-Ingenio 2010, Spain; the Slovak R&D Agency; the Academy of Finland; the Australian Research Council (ARC); and the EU community Marie Curie Fellowship Contract No. 302103.

[1] G. Aad *et al.* (ATLAS Collaboration), Phys. Lett. B **716**, 1 (2012)

[2] S. Chatrchyan *et al.* (CMS Collaboration), Phys. Lett. B **716**, 30 (2012)

[3] T. Aaltonen *et al.* (CDF Collaboration), Phys. Rev. Lett. **109**, 111802 (2012)

[4] V. M. Abazov *et al.* (D0 Collaboration), Phys. Rev. Lett. **109**, 121802 (2012)

[5] T. Aaltonen *et al.* (CDF and D0 Collaborations), Phys. Rev. Lett. **109**, 071804 (2012)

[6] T. Aaltonen *et al.* (CDF Collaboration), Phys. Rev. D **88**, 052013 (2013)

[7] V. M. Abazov *et al.* (D0 Collaboration), Phys. Rev. D **88**, 052011 (2013)

[8] T. Aaltonen *et al.* (CDF and D0 Collaborations), Phys. Rev. D **88**, 052014 (2013)

[9] L. .D. Landau, Dokl. Akad. Nauk Ser. Fiz. **60**, 207 (1948).

[10] C. N. Yang, Phys. Rev. **77**, 242 (1950).

[11] G. Aad *et al.* (ATLAS Collaboration), Phys. Lett. B **726**, 120 (2013)

[12] S. Chatrchyan *et al.* (CMS Collaboration), Phys. Rev. Lett. **110**, 081803 (2013)

[13] J. Ellis, D. S. Hwang, V. Sanz and T. You, JHEP **1211**, 134 (2012)

[14] D. J. Miller, S. Y. Choi, B. Eberle, M. M. Mühlleitner and P. M. Zerwas, Phys. Lett. B **505**, 149 (2001).

[15] T. Aaltonen *et al.* (CDF Collaboration), Phys. Rev. Lett. **109**, 111804 (2012)

[16] T. Aaltonen *et al.* (CDF Collaboration), Phys. Rev. Lett. **109**, 111803 (2012)

[17] T. Aaltonen *et al.* (CDF Collaboration), Phys. Rev. D **87**, 052008 (2013)

[18] T. Sjostrand, S. Mrenna, and P. Skands, J. High Energy Phys. 05 (2006) 026. We use PYTHIA version 6.216 to generate the Higgs boson signals.

[19] H. L. Lai *et al.*, Eur. Phys. J. C **12**, 375 (2000).

[20] J. Baglio and A. Djouadi, JHEP **1010**, 064 (2010) [arXiv:1003.4266 [hep-ph], arXiv:1009.1363 [hep-ph]].

[21] The Fortran program can be found on Michael Spira's web page `http://people.web.psi.ch/~mspira/proglist.html`, using the formulae presented in T. Han and S. Willenbrock, Phys. Lett. B **273**, 167 (1991).

[22] O. Brein, A. Djouadi, and R. Harlander, Phys. Lett. B **579**, 149 (2004).

[23] M. L. Ciccolini, S. Dittmaier, and M. Kramer, Phys. Rev. D **68**, 073003 (2003).

[24] G. Ferrera, M. Grazzini and F. Tramontano, calculation at NNLO," Phys. Rev. Lett. **107**, 152003 (2011).

[25] S. Dittmaier *et al.* [LHC Higgs Cross Section Working Group Collaboration], arXiv:1101.0593 [hep-ph].

[26] S. Dittmaier, C. Mariotti, G. Passarino, R. Tanaka, S. Alekhin, J. Alwall and E. A. Bagnaschi *et al.*, arXiv:1201.3084 [hep-ph].

[27] A. Djouadi, J. Kalinowski, and M. Spira, Comput. Phys. Commun. **108**, 56 (1998).

[28] A. Bredenstein, A. Denner, S. Dittmaier, and M. M. Weber, Phys. Rev. D **74**, 013004 (2006); A. Bredenstein, A. Denner, S. Dittmaier, A. Műck, and M. M. Weber, J. High Energy Phys. 02 (2007) 080.

[29] J. Baglio and A. Djouadi, JHEP **1103**, 055 (2011).

[30] A. Denner, S. Heinemeyer, I. Puljak, D. Rebuzzi, and M. Spira, Eur. Phys. J. C **71**, 1753 (2011).

[31] J. M. Campbell and R. K. Ellis, Phys. Rev. D **60**, 113006 (1999).

[32] S. Moch and P. Uwer, Nucl. Phys. Proc. Suppl. **183**, 75 (2008).

[33] A. D. Martin, W. J. Stirling, R. S. Thorne and G. Watt, Eur. Phys. J. C **63**, 189 (2009).

[34] N. Kidonakis, Phys. Rev. D **74**, 114012 (2006).

[35] M. Mangano, M. Moretti, F. Piccinini, R. Pittau, and A. Polosa, J. High Energy Phys. 07 (2003) 001.

[36] J. Freeman, T. Junk, M. Kirby, Y. Oksuzian, T. J. Phillips, F. D. Snider, M. Trovato and J. Vizan *et al.*, Nucl. Instrum. Meth. A **697**, 64 (2013) [arXiv:1205.1812 [hep-ex]].

[37] D. Acosta *et al.* (CDF Collaboration), Phys. Rev. D **71**, 052003 (2005).

[38] *Statistics*, in K. Nakamura *et al.* (Particle Data Group), J. Phys. G **37**, 075021 (2010).

[39] O. Brein, R. V. Harlander, M. Weisemann, and T. Zirke, Eur. Phys. J. C **72**, 1868 (2012).

[40] A. Bhatti *et al.*, Nucl. Instrum. Methods A **566**, 375 (2006).

[41] S. Klimenko, J. Konigsberg, and T. M. Liss, FERMILAB-FN-0741 (2003).